High-accuracy translation–rotation encoder with two gratings in a Littrow mount

Michel Nevière, Evgeny Popov, Bozhan Bojhkov, Lyubomir Tsonev, and Svetlun Tonchev

A new type of translation–rotation encoder that makes use of two identical transparent dielectric gratings lighted in a −1-order Littrow mount is proposed. The correct choice of the wavelength-to-groove-spacing ratio produces only two transmitted beams, which interfere with the highest possible visibility in a large range of experimental conditions. Thus this mounting permits high-accuracy encoders to be produced by the use of cheap photoresist or plastic gratings and opens the way to industrial applications in high-precision mechanics, information processing, etc. © 1999 Optical Society of America

OCIS codes: 050.0050, 090.2890, 120.0120, 230.0230.

1. Introduction

It is known[1,2] that one can measure interferometrically the relative displacement between a grating (here called the upper grating) and a detection fork composed of a vertically incident beam and a second grating by causing two beams diffracted by the upper grating (e.g., the +1 and −1 orders) to interfere (Fig. 1). If the upper grating moves along an axis Ox normal to the grooves and situated in the mean plane of the upper grating, the +1 order experiences a phase shift φ, given by

$$\varphi = 2\pi(x/d), \tag{1}$$

where x is the displacement and d is the period of the upper grating, while the −1 order experiences a phase shift $-\varphi$. Equation (1) shows that the displacements that will be measured by detection of the interference fringes produced below the second grating are independent of wavelength λ of the incident beam but depend on groove spacing d. Most displacement encoders produced until recently used gratings with periods greater than or equal to 4 μm, which limited the resolution to ~1 μm. Increasing requirements for positioning accuracy of precision machine tools in recent years (e.g., in semiconductor technology and in production of diffractive-optics components) as well as increasing requirements for information storage and reading in compact disks have fueled a demand for encoders with resolutions in the submicrometer range. One might think *a priori* that the classic He–Ne laser interferometers[3] could solve the problem. Despite their long-term wavelength stability,[4] high measuring accuracy requires operating in vacuum; this possibility is precluded in many practical situations, among which are those in which high-precision machine tools and most coordinate measuring devices are used. As soon as measurements in vacuum are precluded, the accuracy of the measurements in air depends strongly on the refractive-index fluctuations.[5] It implies strict control of air pressure, temperature, and relative humidity, which always have local fluctuations. Thus it leads to an accuracy that deteriorates with increasing measurement length. Grating interferometers do not suffer from these inconveniences. In particular, our study brings a solution that is independent of

(i) The wavelength, permitting the use of nonstabilized sources such as light-emitting diodes,
(ii) The environmental parameters (temperature, pressure, relative humidity, etc), and
(iii) The spacing between the moving and the readout gratings.

It also involves a large degree of tolerance of the parallelism of these two elements and in the groove

M. Nevière is with the Laboratoire d'Optique Electromagnétique, Unité Propre de Recherche de l'Enseignement Supérieur Associée, Centre National de la Recherche Scientifique 6079, Faculté des Sciences de St-Jérôme, Case 262, 13397 Marseille Cedex 20, France. The other authors are with the Institute of Solid State Physics, Bulgarian Academy of Sciences, 72 Tzarigradsko Chaussee Boulevard, Sofia 1784, Bulgaria.

Received 6 July 1998; revised manuscript received 21 September 1998.
0003-6935/99/010067-10$15.00/0

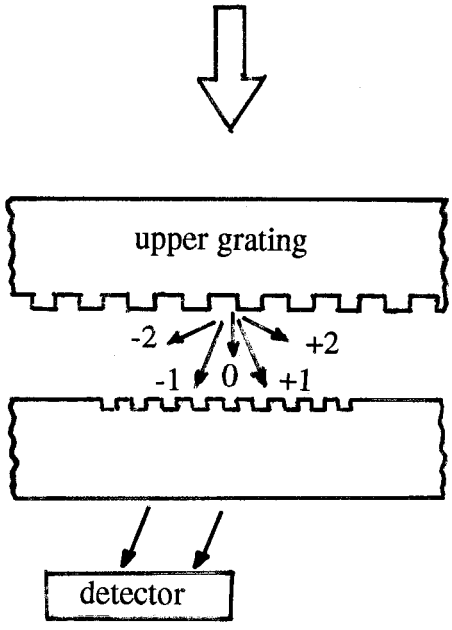

Fig. 1. Grating encoder basic mount.

shape of the gratings, permitting the use of cheap photoresist or plastic gratings. It always provides high visibility of the fringes without requiring equal efficiencies of the two transmitted orders diffracted by the upper grating.

2. Description of the Encoder

The new translation–rotation encoder consists of two identical transmission gratings (see Fig. 2). Their groove shape is symmetric with respect to the normal on the mean plane of the grating. The profile can be any one of the profiles currently used (e.g., sinusoidal, lamellar, trapezoidal). It also can consist of parallel metal rods. Each grating is adjacent to each of the moving parts whose displacement has to be measured, and the two gratings are approximately parallel. The upper grating is illuminated in a -1 order Littrow mounting. This means that the incidence θ is chosen in such a way that the -1 reflected order propagates in the same direction as the incident beam but in the opposite sense. This implies an incidence angle θ, given by

$$\sin \theta = \lambda/2d, \tag{2}$$

where λ is the incident wavelength. The λ/d ratio is chosen in such a way that only two orders propagate in the medium surrounding the two gratings, which implies that $\sin \theta > 1/3$ or $\theta > 19°28'$. Then Eq. (2) leads to $\lambda > 2d/3$. Because Eq. (2) already implies that $\lambda < 2d$, wavelength λ must satisfy

$$2d/3 < \lambda < 2d. \tag{3}$$

This condition implies that only the zeroth and the -1 orders will propagate below the upper grating and that they will fall upon the second grating under the same Littrow condition as in Eq. (2). The result is that, below the second grating, only four orders will propagate, respectively denoted $(-1, 0)$, $(-1, -1)$, $(0, -1)$, and $(0, 0)$, under diffraction angles $\pm\theta$. In practice, the upper grating is illuminated with a beam with finite width D, so the upper grating gives two transmitted beams with the same widths D. These two beams are spatially separated below the upper grating after a vertical distance M_x, given by

$$M_x = D/(2 \sin \theta),$$

and we choose a distance between the two gratings less than this value to create the desired interference. After a vertical distance greater than M_x, the interference patterns of the $(-1, 0)$ and $(0, -1)$ orders on one side, and of the $(-1, +1)$ and $(0, 0)$ orders on the other side, do not overlap and can then be captured by a detector. It is worth noting that no extraparasitic order (e.g., $+1$ or -2 order), which could lower the contrast, propagates. The incident beam must be linearly polarized (TE or TM).

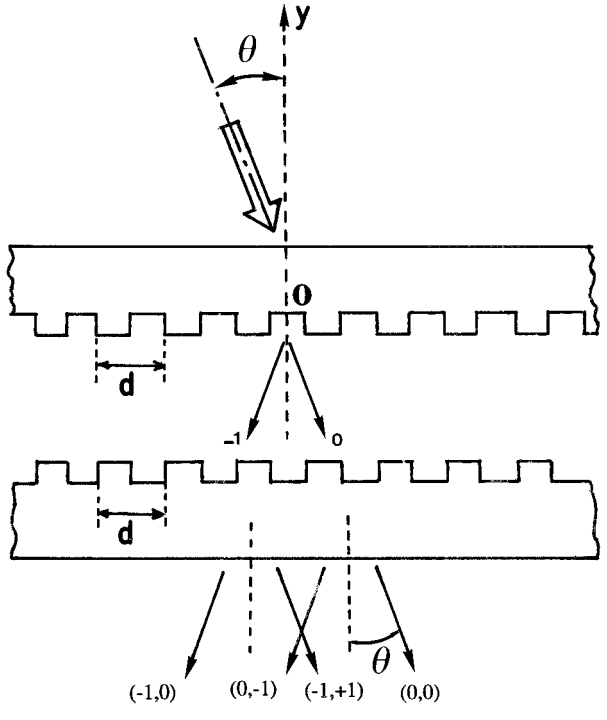

Fig. 2. Schematic representation of the encoder.

3. Interference Pattern

A. Theory

Under the illumination conditions specified above, the upper grating will produce two diffracted orders, with amplitudes T_0 and T_{-1}, which fall upon the second grating under angles of incidence $\pm\theta$. The -1 order falling upon the second grating then produces two transmitted orders with amplitudes $T_{-1,0}$ and $T_{-1,+1}$, whereas the zeroth order gives transmitted orders with amplitudes $T_{0,-1}$ and $T_{0,0}$. Inasmuch as the two profiles are identical and sym-

metrical with respect to the grating normal Oy, we find that

$$T_{-1,0} = T_{-1} \times T_0,$$

$$T_{-1,+1} = T_{-1} \times T_{-1},$$

$$T_{0,0} = T_0 \times T_0,$$

$$T_{0,-1} = T_0 \times T_{-1} = T_{-1,0}.$$

The result is that a detector that receives the interference pattern of the $(-1, 0)$ and $(0, -1)$ orders shows the intensity of the sum of two propagating waves with equal amplitudes and with opposite phases φ and $-\varphi$ given by Eq. (1) when a relative displacement x is produced between the two gratings. Then it is well known[6] that the intensity $\mathcal{N}$ is given by

$$\mathcal{N} = 2|T_{0,-1}|^2(1 + \cos \varphi) \tag{4}$$

and that it varies between the minimum, $\mathcal{N}_{-1,\min} = |T_{-1,0} - T_{0,-1}|^2 = 0$, and the maximum, $\mathcal{N}_{-1,\mathrm{Max}} = 4|T_{0,-1}|^2$. The visibility V, defined by

$$V = \frac{\mathcal{N}_{\mathrm{Max}} - \mathcal{N}_{\min}}{\mathcal{N}_{\mathrm{Max}} + \mathcal{N}_{\min}}, \tag{5}$$

will be optimum (equal to unity), independently of the relative values of the grating efficiencies in the zeroth and the -1 orders. Even for weakly modulated gratings, the contrast will be optimum. On the other hand, the luminosity of the interference pattern depends on the product $|T_0 \times T_{-1}|^2$. Because the sum $|T_0|^2 + |T_{-1}|^2$ is bounded by the energy-balance criterion, it is expected that the luminosity will be maximum when

$$|T_0|^2 = |T_{-1}|^2. \tag{6}$$

This condition can be fulfilled by use of deep gratings with optimized groove shape. However, electronic detection does not require the highest luminosity. Only good visibility is required, which can be obtained with cheap photoresist gratings.

Note that the interference pattern between the $(-1, +1)$ and $(0, 0)$ orders is generally less favorable for use. Indeed, in general, $T_{-1,+1}$ is different from $T_{0,0}$, and the interference pattern's intensity varies between its minimum $\mathcal{N}_{0,\min}$ and its maximum $\mathcal{N}_{0,\mathrm{Max}}$ values:

$$\mathcal{N}_{0,\min} = |T_{0,0}|^2 + |T_{-1,+1}|^2 - 2|T_{0,0}||T_{-1,+1}|,$$

$$\mathcal{N}_{0,\mathrm{Max}} = |T_{0,0}|^2 + |T_{-1,+1}|^2 + 2|T_{0,0}||T_{-1,+1}|.$$

Thus the visibility is given by

$$V = \frac{2|T_{0,0}||T_{-1,+1}|}{|T_{0,0}|^2 + |T_{-1,+1}|^2}. \tag{7}$$

This expression may be far inferior to unity. For example, if the gratings produce transmitted orders with a ratio 10 in their efficiencies,

$$\frac{|T_{-1}|^2}{|T_0|^2} = \frac{1}{10},$$

Eq. (7) leads to $V = 0.18$, and the interference will be hard to use. There is a solution to raise V given by Eq. (7) to unity; it consists of having $|T_{0,0}| = |T_{-1,+1}|$, which implies the equality of transmitted efficiencies stated in Eq. (6). Again, this requires optimized groove shape deep gratings, with the consequence of being costly. Anyway, when such gratings with equal transmitted efficiencies are available, it is worth noting that if the detector receiving orders $(-1, 0)$ and $(0, -1)$ detect an intensity varying as $1 + \sin \varphi$, a second detector, which receives orders $(-1, +1)$ and $(0, 0)$, detects an intensity that varies as $1 - \sin \varphi$, because of the symmetry of the configuration. By use of both measurements it is then possible, with an adequate electronic network, to eliminate random parasitic signals from a hostile environment and thus to improve the visibility of the fringes.

B. Experimental Results

Two pairs of identical sinusoidal photoresist gratings, with a period d equal to 0.85 μm, were produced by holographic recording. The first type, called type A, was characterized by a high modulation ratio (h/d, where h is the groove depth) close to unity. In TE-polarized light (electric-field vector parallel to the grooves), the absolute zeroth and -1 transmitted efficiencies were 32% and 34%, respectively. In TM polarization the energy was unevenly distributed: 45% into the zeroth order and 20% in the -1 order. For the second type (type B) the modulation ratio was ~0.5. In TE polarization the zeroth- and the -1-order efficiencies were 43% and 17%, respectively. All these measurements were done with a He–Ne red laser [with wavelength λ equal to 0.6328 μm and under the Littrow incidence $\theta = 21.85°$ derived from Eq. (2)]. However, a large tolerance on the incidence condition was found; departing from a Littrow mount within ±10° angular deviation changed the efficiencies only within 2%.

Each grating was in fact produced upon a thin glass plate (cut from spectroscopic plates). To avoid the interference pattern that is due to the multiple reflection between the two sides of the thin glass plate, we attached that plate to a 1-cm-thick glass plate by using an immersing liquid, so the beams reflected at the grating and at the flat backside of the plate were separated spatially, thanks to the nonnormal incidence. The two gratings of a given couple, together with the thick glass plates, were mounted upon separate optical micropositioners to permit independent motions for alignment. The second grating was mounted upon a piezocontrolled small table. This table had two perpendicular directions of movement with a full run of ~12 μm, electrically controlled to within 40 nm/V, which permitted a precision of ~50

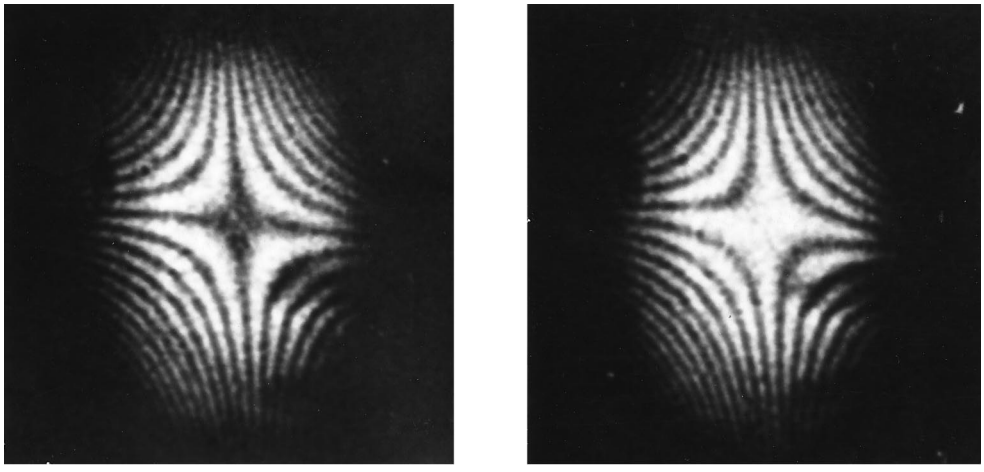

(a) (b)

Fig. 3. Photographs (actual size) of the interference pattern. (a) The gratings are placed to have a minimum in the center of the field; (b) starting from the position defined in (a), the upper grating is translated a $d/2$ distance along the Ox axis.

nm in the relative positioning of the two gratings. This piezotable was mounted upon another micropositioning table, which had several degrees of freedom: It could move in the y direction (note that the x direction lies in the grating plane and is perpendicular to the grooves, the z direction also lies in the grating plane and is parallel to the grooves, and the y direction is perpendicular to the grating plane), could rotate about the z axis to allow for introducing some angle between the grating planes, and could rotate about the y axis. The last-named movement is necessary for making the grooves of the two gratings parallel to each other.

The system was illuminated close to a Littrow mount by a He–Ne laser through a beam expander that produced a beam width of ~18 mm. As we observe below, a beam divergence (or convergence) of as much as 5° was not critical for the results of the experiment. A quantitative investigation of the influence of the beam divergence outside these limits was not carried out because these were the limits of the beam expander to produce nonparallel beams.

The two gratings were mounted face to face, and we made the blanks almost parallel by observing the position of the diffracted spots. After that, the second grating was slowly rotated about the y axis (perpendicular to the grating plane) to ensure parallelism of the grooves. Because the recording beams were slightly divergent, the grooves were not straight; thus parallelism was obtained in a relatively small zone with a 7-mm radius, which corresponds to the central part of Fig. 3(a). This figure clearly shows the existence of curved grooves. Experiment has shown that the precision of the alignment of the grooves in parallel must be greater than 3×10^{-5} rad for a zero-interference spot larger than 5 mm.

After positioning at the zero point of the interference pattern, the upper grating was translated a distance $d/2$ along the Ox axis situated in the mean plane of that grating and normal to the grooves. The interference pattern was changed into the one in Fig. 3(b). Comparison of Figs. 3(a) and 3(b) shows that the dark areas were turned into bright ones and vice versa.

A small 3-mm-diameter detector was then put in the central part of the interference pattern, and its signal was recorded while the upper grating was moved along the Ox axis. Figure 4 shows the result. It represents the intensity of the interference field produced by the $(-1, 0)$ and $(0, -1)$ orders with the gratings of type B, which had 43% and 17% efficiencies in the zeroth and the -1 orders, respectively. The intensity varied from 3 to 15 μW, which led to a measured visibility of 67%. As expected, the visibility was high despite the great difference in grating efficiencies. The period of the signal was 850 nm, which was the period of the grating. It is worth noting that the same signal will be recorded whatever the location of the small detector in the interference field may be. On the other hand, the interference pattern obtained with the $(-1, +1)$ and $(0, 0)$ orders produced a signal that oscillated from 20 to 38 μW, leading to a poor visibility of 0.31. The reduction in visibility observed when experiments were compared with theory comes mainly from the nonnegligible detector size compared with the width of the fringes of the interferogram. Thus the detector integrates the intensity over the size of its aperture instead of detecting the exact minima and maxima. We also made other measurements by replacing a grating of type B with a grating of type A. Table 1 lists both the experimental results and the predicted visibility given by Eq. (7).

One can see that, as soon as the $(-1, 0)$ and $(0, -1)$ orders are used, high visibility can be obtained for both types of grating, whatever the values of their transmitted efficiencies may be. On the other hand, the use of the $(-1, +1)$ and $(0, 0)$ orders leads to high visibility only for gratings of type A, for which the transmitted efficiencies are equal. Indeed, because

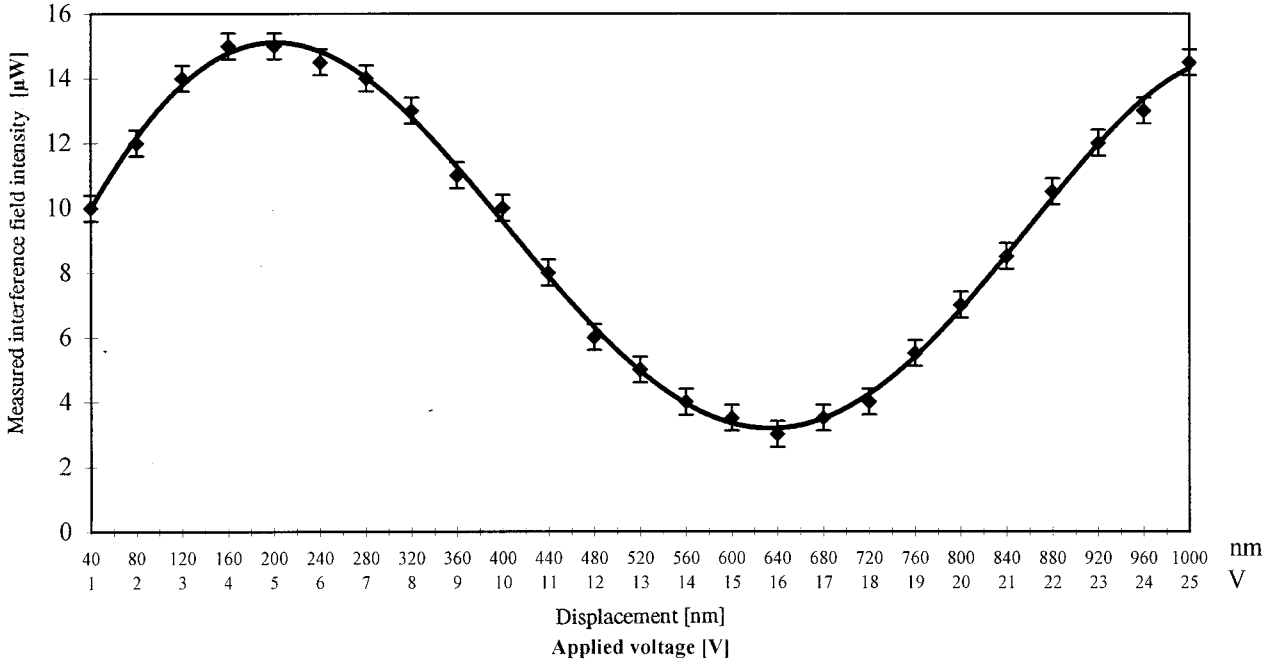

Fig. 4. Measured intensity at the center of the interference pattern as a function of displacement x and of corresponding voltage V of the piezoelectric table.

of the Littrow incidence and equal refractive indices of the superstrate and the substrate, we obtained $T_0^2 = 0.32 = T_{0,0}$ and $T_{-1}^2 = 0.34 = T_{-1,-1}$. Thus Eq. (7) gives a theoretical visibility of 0.998. In all cases there is an important difference between the predicted visibility and the measured one, which points out the need to use a better detector. An array of photodiodes placed anywhere in the interference pattern could permit processing the signal and suppressing random signals coming from a hostile environment.

The tolerance with respect to the parallelism of the grating plates, i.e., between the moving planes, was also studied and turned out to be large. It was observed that the interference pattern is not disturbed if the second grating is rotated about its z axis to within 1° in both directions, i.e., within 3.5×10^{-2} rad. This large tolerance is explained by the facts that the incidence is the Littrow incidence and that the difference between the directions of the rays diffracted by the gratings when they are not parallel is much smaller than the angle between the blanks, as can be established from the Fraunhofer equation (see Appendix A).

The interference pattern shown in Fig. 3 was not changed when the second grating was moved in the direction of the y axis (perpendicular to the surface). A small-scale movement was ensured by the piezoelectric table; and a large-scale movement (as much as 10 mm), by the supporting table. When the gratings were separated by a distance greater than 15 mm the interference pattern disappeared as a result of the spatial separation between the beams that were assumed to interfere.

A last experiment was done with a different light source. Together with the He–Ne laser, a much cheaper semiconductor diode laser (from a laser pointer), with wavelength of 675 nm, was used. Using a semitransparent mirror, we combined the two laser beams to compare the interference patterns under similar conditions. There were only two notice-

Table 1. Comparison of the Interference Signals Produced by the Two Kinds of Interference Field for the Two Types of Grating

		Grating Type	
Numbers of Interfering Orders	Interference Signal Power	Grating A	Grating B
(−1, +1) and (0, 0)	Minimum	5 μW	20 μW
	Maximum	40 μW	38 μW
	Measured Visibility [Eq. (4)]	0.78	0.31
	Theoretical Visibility [Eq. (7)]	0.998	0.68
(−1, 0) and (0, −1)	Minimum	5 μW	3 μW
	Maximum	35 μW	15 μW
	Measured Visibility [Eq. (4)]	0.75	0.67
	Theoretical Visibility [Eq. (7)]	1	1

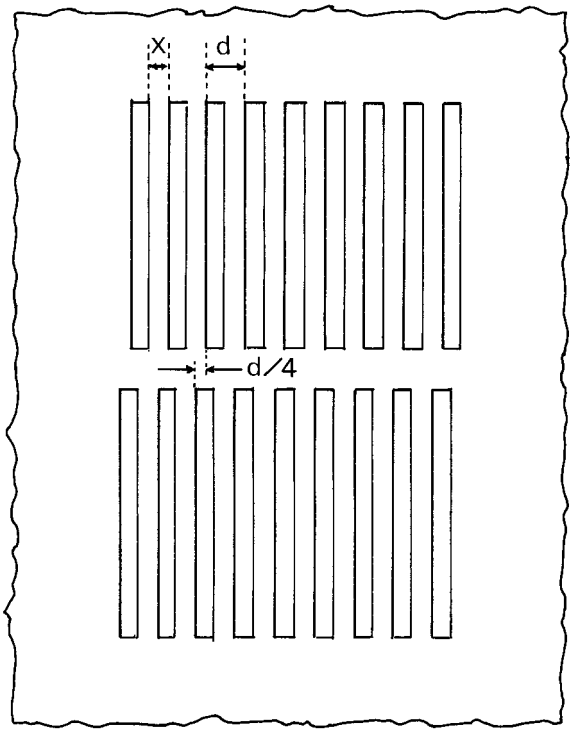

Fig. 5. View from the top of the lower mobile element on which two shifted identical gratings are engraved, a second grating is engraved with $d/4$ translation along the x axis, and there is a shift in the ruling direction large enough that the two rulings do not overlap.

able differences between the two wavelengths used: the -1- order position was shifted because of the grating dispersion and because the beam-spot distribution of the diode laser was disturbed owing to its resonator parameter. Otherwise, minima and maxima were observed simultaneously at both wavelengths, pointing to a weak spectral dependence of the device properties.

4. Determination of the Sense of the Displacement

In the version presented so far, the relative displacement x between the two moving parts is deduced from Eq. (1), and φ is determined from an interferogram whose intensity is given in Eq. (4). Thus the sign of x, i.e., the sense of the displacement, is unknown. The present device gives access only to the length of the displacement. It can thus be useful to measure the velocity of the displacement, on top of its amplitude.

When the sense of the displacement is required, the device can be completed in the following way: A third grating, identical to the two previous ones, is added upon the surface of the element in which the lower grating in Fig. 2 is engraved. However, the third grating is translated along the z direction of the grooves in such a way that the rulings of the two lower gratings do not overlap. Moreover, the third grating is translated along the x direction normal to the rulings in the lower grating plane by a distance equal to $d/4$. Figure 5 shows a top view of the relative positions of the two lower gratings. The incident beam is assumed to have a width in the z direction that is large enough to illuminate the two lower gratings. A second detector is placed in such a way as to receive the interference pattern of the $(-1, 0)$ and $(0, -1)$ orders produced by the second lower grating. It follows from the $d/4$ shift that, when the first detector, which analyzes the interference pattern of the $(-1, 0)$ and $(0, -1)$ orders of the first lower grating, receives an intensity that varies as shown in Eq. (4), the second detector receives an intensity $\mathcal{N}'$, given by

$$\mathcal{N}' = 2|T_{0,-1}|^2\left[1 + \cos\frac{2\pi(x + d/4)}{d}\right] = 2|T_{0,-1}|^2(1 - \sin\varphi). \quad (8)$$

Equations (4) and (8) permit φ to be determined in a unique way: Displacement x is deduced from Eq. (1).

5. Elimination of Random Noise

As established in Section 3, the use of the interference pattern that results from the $(-1, 0)$ and $(0, -1)$ orders always produces optimal visibility, whereas this is not so, in general, for the interference pattern that results from the $(-1, +1)$ and $(0, 0)$ orders. As we have already pointed out, there is a solution that will raise the latter pattern's visibility to unity, which consists of having

$$|T_{0,0}| = |T_{-1,+1}|. \quad (9)$$

If we denote the amplitudes of the transmitted orders of the second grating T_0', T_{+1}', and T_{-1}', by definition we have

$$T_{0,0} = T_0 \times T_0', \quad (10)$$

$$T_{-1,+1} = T_{-1} \times T_{+1}'. \quad (11)$$

Thus there are several ways to satisfy Eq. (9), which we discuss in detail in this section.

A. Use of Identical, Symmetric Profiles

As soon as the second grating has a profile that is symmetric with respect to the normal on the mean plane, $T_{+1}'(-\theta) = T_{-1}'(\theta)$; moreover, because the two gratings are identical, $T_{-1}'(\theta) = T_{-1}(\theta)$ and $T_0' = T_0$. Thus Eqs. (10) and (11) lead to

$$T_{0,0} = (T_0)^2, \quad (12)$$

$$T_{-1,+1} = (T_{-1})^2 \quad (13)$$

and Eq. (9) is satisfied as soon as we have

$$T_0 = T_{-1}. \quad (14)$$

Again, there are several ways to arrive at that solution, assuming the working conditions stated by Eq. (2) and inequality (3). The first way[7,8] consists of using gratings made with metal rods and lighted in TE polarization. The nature of the metal has little

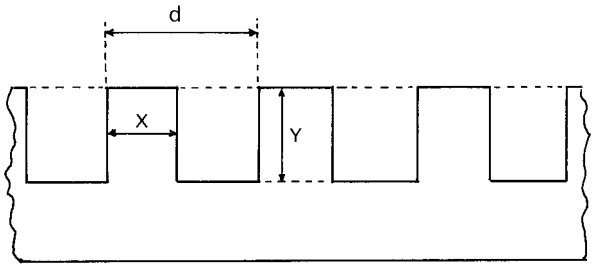

Fig. 6. Groove geometry of a dielectric lamellar grating.

significance as soon as the groove depth is high enough. Equation (14) is well satisfied in the case of a rod grating with a rectangular section when the width X of the dielectric medium between the rods satisfies $\lambda/2N < X < \lambda/N$, where N is the refractive index of the dielectric. A recent paper[9] has shown that the equality between T_0 and T_{-1} can also be obtained in TM polarization if $X < \lambda/2N$, although this solution leads to poor luminosity when X approaches zero. A completely different approach[2] consists of using deep lamellar dielectric gratings, whose groove depth Y and bump width X, illustrated in Fig. 6, have been conveniently determined. With computer codes founded in the electromagnetic theory of gratings[10] it has been established that, in TE polarization, the optimal values of the normalized groove depth Y/λ are located upon the curve shown in the center of the hatched area in Fig. 7. This curve consists of two parts (A and B), which meet at a point ($X1$, $Y1$), with $X1 = 0.593$ and $Y1 = 1.039$. Part A has the following equation:

$$Y/\lambda = 8.399(X/\lambda)^2 - 6.616(X/\lambda) + 2.009, \quad (15)$$

with

$$X/\lambda \in [0.40, X_1];$$

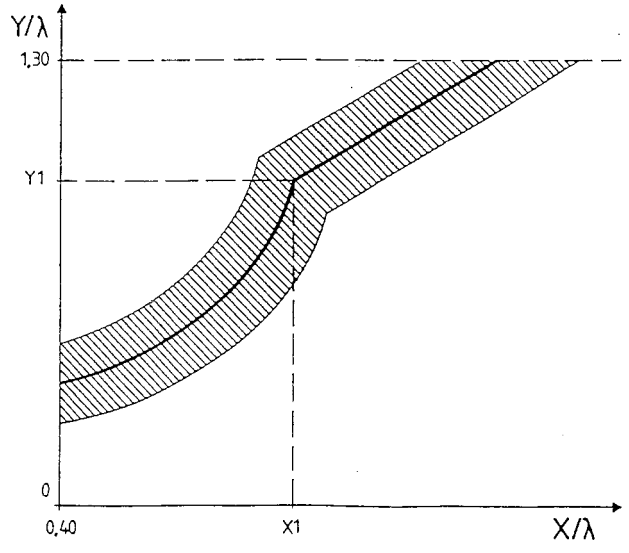

Fig. 7. Optimal groove depth and groove width of a dielectric lamellar grating to produce equal transmitted efficiencies.

part B has the equation

$$Y/\lambda = 1.039(X/\lambda) + 0.423, \quad (16)$$

with

$$Y/\lambda \in [Y_1, 1.3].$$

When Eq. (15) or (16) is satisfied, the amplitudes of the two transmitted orders are equal. Moreover, it has been established that in the hatched region in Fig. 7 delimited by curves parallel to the heavy curve the sum of the transmitted efficiencies is greater than 0.8, whereas their relative difference is less than 20%, which permits the tolerance on the optimized grating manufacturing to be estimated. The boundaries of the hatched region are defined by six equations:

$$Y/\lambda = 8.679(X/\lambda)^2 - 6.851(X/\lambda)^2 + 2.113,$$

$$Y/\lambda = 0.974(X/\lambda) + 0.514,$$

$$Y/\lambda = 8.120(X/\lambda)^2 - 6.381(X/\lambda) + 1.905,$$

$$Y/\lambda = 1.039(X/\lambda) + 0.383,$$

$$X/\lambda = 0.40,$$

$$Y/\lambda = 1.30.$$

We recall that these results hold for TE polarization. It is likely that convenient domains of groove depth and groove width can also be found in TM polarization, but because the choice of the polarization is usually open we have limited our effort to the study of TE polarization.

To conclude this section, let us point out that, independently of the path that has been followed to yield a symmetric grating with equal transmitted efficiencies, the use of identical gratings has ensured that the $(-1, +1)$ and $(0, 0)$ orders produced an interference phenomenon with the same visibility as the one given by the $(-1, 0)$ and $(0, -1)$ orders. Thus, as we already pointed out at the end of Subsection 3.A, by combining measurements obtained with the two interference patterns, which vary as $1 + \sin\varphi$ and $1 - \sin\varphi$, we can then use signal processing to eliminate random noise or any parasitic signals that could arise from hostile environment. Figure 8 shows a detailed view of the complete mounting. The second grating illustrated in Fig. 5, as well as the two corresponding detectors, are not represented in this figure.

B. Use of Nonidentical Gratings with Symmetrical Profiles

The use of two identical gratings is, of course, the easiest solution for a manufacturer who would like to produce the encoder. However, one can arrive at the same result as in Subsection 5.A with two symmetrical profiles but different gratings, each grating being optimized so the gratings have equal transmitted efficiencies. For example, one may combine a metal-rod grating used in TE polarization with $\lambda/2N < X <$

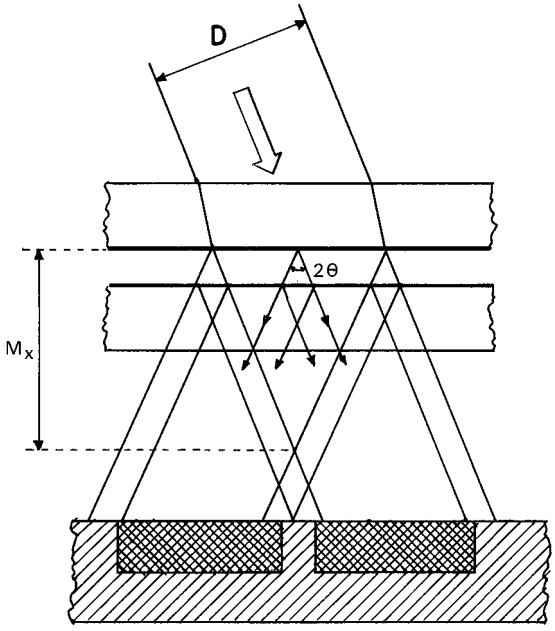

Fig. 8. Mounting for eliminating parasitic signals. Heavier lines represent the two gratings. Hatched areas are two detectors.

λ/N and a deep dielectric grating optimized as shown in Fig. 7. It is assumed only that $T_0 = T_{-1}$ and that $T_0'(\theta) = T_{-1}'(\theta)$. The symmetry of the profile gives $T_{+1}'(-\theta) = T_{-1}'(\theta)$, and Eqs. (10) and (11) lead to

$$T_{0,0} = T_0 T_0',$$

$$T_{-1,+1} = T_{-1} T_{+1}'(-\theta) = T_{-1} T_{-1}' = T_0 T_0'.$$

Moreover,

$$T_{-1,0} = T_{-1} T_0' = T_0 T_0', \tag{17}$$

$$T_{0,-1} = T_0 T_{-1}' = T_0 T_0'. \tag{18}$$

Here, too, the two interference systems are produced with equal-intensity beams. The visibility is optimum, and all the conclusions of Subsection 5.A apply. On the other hand, if one moves to gratings with asymmetric profiles, identical or not, it is not possible to obtain interferences with equal-intensity beams, even in the $(-1, 0)$ and $(0, -1)$ interference pattern. This result is linked with the fact that, contrary to what happens for the zeroth reflected order, in transmission we have $T_0'(-\theta) \neq T_0'(\theta)$. Also, $T_{+1}'(-\theta) \neq T_{-1}'(\theta)$. Thus Eqs. (10) (11) and Eqs. (17) and (18) lead to different intensities.

6. Extension to the Detection of Rotation Motion

Although the device has been described in detail from the viewpoint of detecting a translation motion, its extension to the detection of rotation motion is straightforward. It suffices to replace the two classic linear gratings by gratings ruled upon rings, with the groove direction through the centers of the rings, as illustrated in Fig. 9. The centers of the rings have to be located on the axis of the rotation motion.

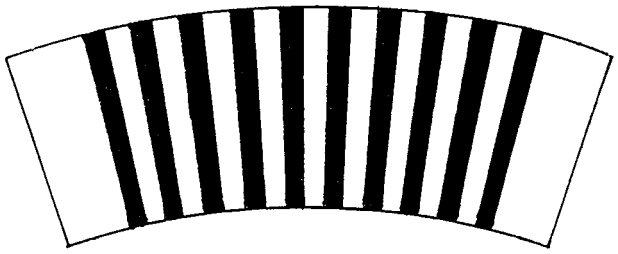

Fig. 9. Schematic of gratings used to detect rotation motion.

7. Discussion of the Results

To understand fully the potentialities of the new device, one has to keep in mind that the experimental results of Subsection 3.B were obtained not with good gratings produced by a manufacturer but with poor gratings that anyone can produce in a lab. Because the recording beams were slightly divergent, the grooves are not straight, and the interference field illustrated in Fig. 3(a) is far different from the flat field that would be obtained with straight grooves. Anyway, the device works. Moreover, the detector has a 3-mm input diameter, whereas an ideal detector should be infinitely small. The result is that it averages the field intensity on the input surface instead of detecting the exact value at a given point. This is the main reason that explains the discrepancy between the measured visibility (0.75) and the theoretical visibility (1). However, with 0.75 or 0.78 visibility, as shown in Fig. 4, it is possible to measure displacements as small as 0.08 μm, corresponding to $d/10$. This resolution could easily be pushed to 0.04 μm by use of 2400-groove/mm gratings, which are easy to produce nowadays by holography. Such a technique avoids pitch errors and allows gratings to be produced with widths greater than 10 cm, which give the corresponding maximum displacement. For longer displacements, gratings with 40-cm widths have already been produced, some of them with 6000 grooves/mm for the Far Ultraviolet Spectroscopic Explorer mission,[11] which push the resolution to 0.017 μm. We realize that such gratings are expensive, but only copies of a master are required. Let us point out that the use of copies of the same grating eliminates the perturbation that would be introduced by use of two gratings with slightly different pitches. A further improvement could be made in the detection. In the simple version that we proposed, a punctate detector placed in the central area in which a flat field is obtained is sufficient to record the measurements in Fig. 4, through which the least-mean-squares method permits the cosinusoid described by Eq. (4) to be drawn. The displacement is then measured by fringe counting. No calibration is required, and the uncertainly intervals of the measurement, linked with the classic accuracy of photometric measurements and with laser fluctuations, have a negligible influence on the accuracy of measured displacement. In an improved version the punctual detector can be replaced by a photodiode

array placed anywhere in the interference field, with a suitable electronic to process the signal. But this is the classic signal treatment, which is beyond the scope of this paper.

8. Conclusion

A new translation–rotation encoder has been proposed. It has been proved to work under conditions of large tolerance. First, by use of the interference pattern between the $(-1, 0)$ and the $(0, -1)$ transmitted orders it is possible to obtain high visibility with a large variety of transmission gratings without requiring particular specifications of their groove shape. This permits using cheap photoresist or plastic gratings. Second, any kind of light (TE- or TM-polarized light) can be used, and a cheap semiconductor diode can be used as the source. Third, there are wide degrees of tolerance of incident conditions, of the degree of parallelism of the gratings, and of the distance between their mean planes. Despite these large tolerances, the device is able to detect displacements of $\sim d/10$, i.e., $\sim$80 nm in our cases, and even shorter displacements when d is reduced in the range stated in inequality (3). More-sophisticated profiles permit parasitic signals coming from hostile environments to be eliminated. Thus the proposed device has a great potential for high-technology public applications. It is patented in France under patent number 9,805,729 (6 May 1998).

Appendix A: Angular Deviation Caused by the Nonparallelism of the Grating Planes

Let us imagine that the incident beam falls upon the first grating in a Littrow mount at angle θ_L, given by

$$\sin \theta_L = \lambda/2d, \tag{A1}$$

where d is the groove period and λ is the incident wavelength. If the gratings are not parallel, with the angle between their x axes equal to α_1 as illustrated in Fig. 10, then the zeroth order of the first gratings falls upon the second grating under incidence θ_1:

$$\theta_1 = \theta_L + \alpha_1 \tag{A2}$$

and is diffracted by the second grating in its -1 order in direction θ_2 with respect to the second grating normal, $O'y'$, given by the grating equation

$$\sin \theta_2 = \frac{\lambda}{d} - \sin \theta_1, \qquad \theta_2 > 0. \tag{A3}$$

Thus this beam makes an angle θ_2' with the normal Oy to the first grating, given by $\theta_2' = \alpha_1 + \theta_2$. Let us introduce

$$\alpha_2 = \theta_L - \theta_2; \tag{A4}$$

we obtain

$$\theta_2' = \theta_L + \alpha_1 - \alpha_2.$$

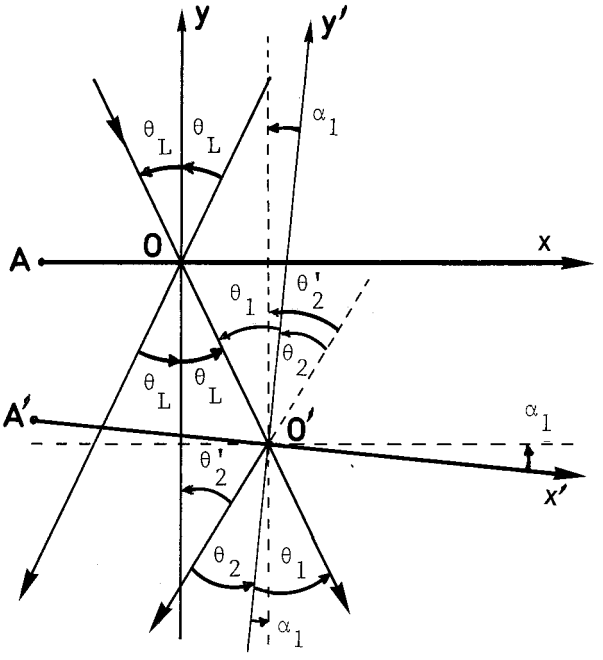

Fig. 10. Angular deviation of the $(-1, 0)$ and $(0, -1)$ beams owing to a tilt of the second grating.

This beam will interfere with the -1 beam diffracted by the first grating order (which is transmitted as a zeroth order by the second grating), propagating in direction θ_L (with respect to the y axis), so period I of the interference pattern will depend on the difference $\alpha_1 - \alpha_2$ (Ref. 6):

$$2 \sin \frac{\alpha_1 - \alpha_2}{2} = \frac{\lambda}{I}. \tag{A5}$$

Equation (A5) shows that, if $\alpha_1 = 0 = \alpha_2$, $I \to \infty$ and the interference field is uniform if the gratings have perfect, rectilinear, parallel grooves. At a given point of the field where we place the detector, the intensity of the field will vary if a translation of a grating occurs, as was illustrated in Fig. 4. Introduction of a nonparallelism produces interference fringes. However, the value of $\alpha_1 = 1°$ with $\lambda = 632.8$ nm and $d = 0.85$ μm inserted into Eqs. (A3)–(A5) results in $I = 5$ mm; i.e., the interference picture has a period of 5 mm, which does not disturb the measurements significantly.

This large tolerance can be understood when we remark that, because of the Littrow incidence, the rotation of the -1 transmitted order is null up to second order when incidence θ_1 is increased by $d\theta_1$, starting from θ_L. If, starting from parallel gratings, we rotate the lower grating by an infinitely small angle α_1, we get $d\theta_1 = \alpha_1$. Differentiating Eq. (A3) leads to

$$\cos \theta_2 d\theta_2 = -\cos \theta_1 d\theta_1.$$

Because before rotation $\theta_1 = \theta_L = \theta_2$, we obtain $d\theta_2 = -d\theta_1$. Thus $d\theta_2 = -\alpha_1$, which shows that the -1

order diffracted by the second gratings maintains a fixed position with respect to the y axis.

References

1. J. Heidenhain, M. Allgaüer, and E. Spanner, "Measurement set-up," German patent EP 92 11 0237.2 (17 June 1992).
2. O. Parriaux, M. Nevière, and E. Popov, "Dispositif optique de mesure d'un déplacement relatif entre deux éléments," European patent EP 07 41 282 A2 (30 April 1996).
3. C. R. Steinmetz, "Sub-micron position measurement and control on precision machine tools with laser interferometry," Precision Eng. **22,** 513–519 (1990).
4. R. J. Hocken and H. P. Layer, "Lasers for dimensional measurement," Ann. CIRP **28,** 303–309 (1979).
5. W. T. Estler, "High-accuracy displacement interferometry in air," Appl. Opt. **24,** 808–815 (1985).
6. M. Born and E. Wolf, *Principles of Optics* (Pergamon, New York, 1965).
7. J. L. Roumiguières and M. Nevière, "Process for casting on a support the faithful reproduction of a mask pierced with periodically distributed slits," Japanese patent 1,625,035 (29 August 1980); United States patent 4,389,094 (21 June 1983); Canadian patent 1,140,373 (1 February 1983).
8. F. Montiel and M. Nevière, "Electromagnetic study of a photolithography set-up for periodic masks and application to non-periodic masks," J. Opt. Soc. Am. A **13,** 1429–1438 (1996).
9. A. Sentenac and D. Maystre, "Symmetry of the field transmitted by metallic grids," J. Mod. Opt. **45,** 785–797 (1998).
10. D. Maystre, "Integral Methods," in *Electromagnetic Theory of Gratings*, R. Petit, ed. (Springer-Verlag, Berlin, 1980), pp. 63–100.
11. R. Grange, V. Dauer, M. Saïsse, M. Nevière, J. Flamand, and F. Bonnemasson, "6000 groove/mm holographic flight gratings for the high resolution Far Ultraviolet Spectroscopic Explorer: efficiency, resolution and stray-light measurements," in *Theory and Practice of Surface-Relief Diffraction Gratings: Synchrotron and Other Applications*, W. R. McKinney and C. A. Palmer, eds., Proc. SPIE **3450** (to be published).